Processing and Application of Ceramics 13 [1] (2019) 89–97
https://doi.org/10.2298/PAC1901089O

Shungite – a carbon-mineral rock material: Its sinterability and possible applications

Nina Obradović[1,*], Mihajlo Gigov[2], Aleksandar Đorđević[3], Frank Kern[4], Svetlana Dmitrović[5], Branko Matović[5], Antonije Đorđević[6,7], Ani Tshantshapanyan[8], Branislav Vlahović[8], Predrag Petrović[9], Vladimir Pavlović[1]

[1]*Institute of Technical Sciences of SASA, Knez Mihailova 35/IV, Belgrade, Serbia*
[2]*Mining Institute Ltd., Batajnički put 2, Belgrade, Serbia*
[3]*Faculty of Science, Department of Chemistry, Biochemistry and Environmental Protection, University of Novi Sad, Trg Dositeja Obradovica 3, Novi Sad, Serbia*
[4]*Universität Stuttgart, Institut für Fertigungstechnologie Keramischer Bauteile, D-70567 Stuttgart, Germany*
[5]*University of Belgrade, Vinča Institute of Nuclear Sciences, Mike Petrovića Alasa 12-14, Belgrade, Serbia*
[6]*School of Electrical Engineering, University of Belgrade, Bulevar kralja Aleksandra 73, Belgrade, Serbia*
[7]*Serbian Academy of Sciences and Arts, Knez Mihailova 35, Belgrade, Serbia*
[8]*North Carolina Central University, Department of Mathematics and Physics, Durham, United States*
[9]*Faculty of Technical Sciences, University of Kragujevac, Svetog Save 65, Čačak, Serbia*

Received 9 October 2018; Received in revised form 25 December 2018; Received in revised form 8 February 2019; Accepted 25 February 2019

Abstract

The paper presents results of the influence of mechanical activation of shungite, a carbon-mineral rock material rich in silica and carbon, on its sintering behaviour, and obtaining of pure SiC ceramics. The mechanical activation of the starting powder was performed in a high-energy ball mill in time intervals from 30 to 480 min. The phase composition of the starting powders and sintered samples was analysed by the X-ray diffraction method. The first traces of SiC were detected after sintering at 1350 °C for 2 h in an Ar atmosphere, along with traces of unreacted SiO_2. The scanning electron microscopy was performed in order to determine changes in the microstructure. Sintering was performed at various temperatures for 2 h, in an Ar atmosphere and a vacuum. Dielectric properties of the sintered samples were measured in the frequency range from 1 to 500 MHz. The obtained results indicate that the sintered powder is a good candidate for applications as an absorber of electromagnetic waves in microwave engineering.

Keywords: *mechanical activation, XRD, SEM, sintering, carbon-mineral rock material*

I. Introduction

Shungite, a carbon-mineral rock material of the Precambrian age found in the north-west part of Russia, attracts much attention due to possibilities of application in various industrial and medical fields [1]. Carbon acts as an efficient catalyst for hydrogenation at low temperatures, as an adsorbent and filter in water purification processes, and as a multifunctional filler of polymeric and inorganic binders. Also, it can be used as the basic radiation screening constituent of construction materials and in electro-thermal processes in the production of various alloys and ceramics [2–6]. In the literature, there are few papers about the possibility of carbo-thermic reduction of silica resulting in the formation of silicon carbide or metallic silicon [7,8]. The efficiency of using this carbon-mineral rock material (CMRM) is stipulated by the high range of its valuable properties (absorption, catalytic, regenerative, conductive), high environmental safety with relatively low cost of produced materials based on shungite, as well as the existence of the ex-

* Corresponding author: tel: +381 69 125 0603,
e-mail: *nina.obradovic@itn.sanu.ac.rs*

tensive raw material base of shungite deposit. All these factors contribute to the further expansion of shungite and a great variety of materials based on it [9].

The process of mechanical activation as pre-sintering powder preparation is commonly used in ceramic processing in order to produce homogeneous mixtures, with uniform distribution of powder particles, to increase specific surface areas of particles, to make them more reactive and capable of new phase formation, and, finally, to decrease the sintering temperatures [10]. Furthermore, this low-cost method has more advantages compared to other powder processing routes, such as a shorter time of preparation, simplicity of the method itself, and possibility of obtaining large quantities of the powder. Gubernat *et al.* [11] used milling with a rotating-vibrational mill in ethanol and further conventional sintering of silicon carbide in the temperature range 1500–1600 °C.

In this paper, the authors investigated the physicochemical properties of CMRM during high-energy ball milling. Also, changes in the phase composition and microstructure have been studied in detail, in the starting powders as well as in the sintered samples, along with electrical properties.

II. Experimental procedure

CMRM (Shungite), used in these experiments, was mechanically activated by grinding in a high-energy planetary ball mill with 400 rpm (Fritsch Pulverisette 5). ZrO_2 vessels and balls (5 mm in diameter) were used with the powder-to-balls mass ratio of 1 : 40. The milling process was performed in air for 30, 60, 240, and 480 min. The powders were sieved after milling. The samples were denoted as Sh-0, Sh-30, Sh-60, Sh-240, and Sh-480 (according to the activation time).

The X-ray powder diffraction patterns were obtained using a Philips PW-1050 diffractometer with Cu-K_α radiation and a step/time scan mode of 0.05°/s. The measurements were performed at room temperature in an air atmosphere. The average particle size and particle size distribution were determined by a laser light-scattering particle size analyser (PSA). The used instrument was Mastersizer 2000 (Malvern Instruments Ltd., UK) particle size analyser based on laser scattering, covering the particle size range of 0.02–2000 μm. For the PSA measurements, the powders were dispersed in distilled water, in an ultrasonic bath (low-intensity ultrasound, at a frequency of 40 kHz and power of 50 W), for 5 min. The powder morphology after the mechanical activation was characterized by scanning electron microscopy (JEOL JSM-6390 LV). The powders were covered with gold in order to perform these measurements. Raman spectra of all powders, recorded in the 0–3500 cm^{-1} range, were collected with a LabRAM HR Evolution system which employed Cobolt Blues™ 473 nm solid state laser with a power of 1 mW at the sample surface. All the measurements were realized using a spectrometer equipped with a grating having 1800 lines/mm, a 100× microscope objective and acquisition of 20 s/10 cycles.

The differential thermal analysis with thermal gravimetry (TGA/DTA) was carried out simultaneously using an SDT 2960 thermobalance TA instrument, with alumina crucibles. The heating rate up to 1400 °C in an Ar atmosphere, and up to 900 °C in air, was 10 °C/min.

Powders were pressed into 16 mm discs in a vacuum under a pressure of 150 MPa. The first set of prepared samples was sintered non-isothermally up to 800 °C in an Ar atmosphere, followed by sintering at 1500 °C in Ar (PTF tube furnace, Protherm Electrical Furnaces, made in Turkey), and at 1700 °C in a vacuum (vacuum furnace, Carbolite Gero, made in Germany), for 2 h, with a 10 °C/min heating rate. The second set of samples was sintered non-isothermally up to 800 °C in an Ar atmosphere, followed by sintering at 1350 and 1450 °C in Ar, and at 1850 °C in a vacuum, for 2 h, with a 10 °C/min heating rate. Densities of the sintered samples were measured by the conventional method, using a micrometer screw gauge for determination of the height and diameter, and analytical balance for mass measurements. In the notation of the sintered samples the second number indicate the final applied sintering temperature.

The measurements of the relative permittivity and the loss tangent of the sintered samples were performed using an Agilent E5061A network analyser, in the frequency range between 1 and 500 MHz. The samples were placed in a coaxial test chamber [12]. The reflection coefficient of the chamber was measured by the analyser and the relative complex permittivity of the samples was extracted using electromagnetic models.

III. Results and discussion

The chemical composition of the initial carbon-mineral rock material, determined by atomic emission spectroscopy, is presented in Table 1. It consists mainly of SiO_2, over 52 wt.%, and the rest of initial sample is C, Fe_2O_3, Al_2O_3 phases etc.

XRD patterns of the starting powder and mechanically activated powders are presented in Fig. 1. The diffraction pattern for Sh-0 powder shows the presence of the starting components α-SiO_2, Fe_2O_3, carbon C, α-Al_2O_3, γ-Al_2O_3, and $CaCO_3$. All the obtained intensities were identified by JCPDS cards (086-1628 for

Table 1. Chemical composition of Sh-0 powder

Composition [wt.%]										
SiO_2	Fe_2O_3	Al_2O_3	CaO	MgO	SO_3	P_2O_5	TiO_2	Na_2O	K_2O	LoI*
52.43	2.17	3.85	1.23	0.95	0.79	0.09	0.26	0.10	0.23	36.76

*LOI - loss of ignition

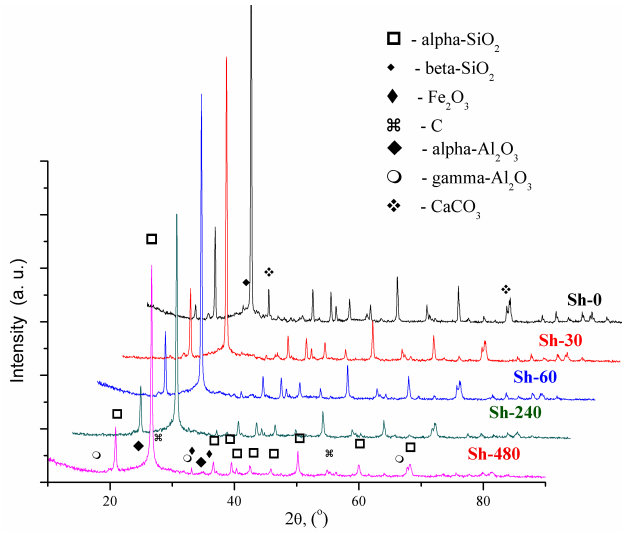

Figure 1. XRD patterns of the starting powder and mechanically activated powders

alpha-SiO_2, 085-0987 for Fe_2O_3, 026-1080 for C, 089-7717 for α-Al_2O_3, 011-0517 for γ-Al_2O_3, and 085-1108 for $CaCO_3$). However, the intensities of some peaks decreased with the activation time, while some peaks slightly broadened. It indicated on the possible crystal lattice destruction and amorphization or particle size reduction, and strain introduction. Some of the phases were not present in the mechanically activated powders, but only in the initial one. Some $CaCO_3$ peaks may have not completely disappeared during the activation process for 30 min, but their concentration in the mixtures was too low to be detected using this technique. If we take into account the fact that no new phases were detected, we can assume that the initial powder was so hard that only minor changes are visible during the prolonged grinding, due to great hardness of the SiO_2 powder, which makes the majority of all powders (the crystal lattice energy is 13.125 kJ/mol) [13].

The results of the particle size analysis of the starting powder and mechanically activated powders, as volume and number *vs.* particle size, are presented in Fig. 2. The distribution of the initial powder indicates large agglomerates with size of 15 μm, and larger. The mechanical activation for 30 and 60 min led to a decrease in the particle size and the appearance of two fractions, a larger one with particles approximately 1.5 μm in size, and a smaller one, with agglomerates as in the starting powder. However, due to the prolonged milling time and secondary agglomeration, in the samples activated for 240 min and more, the ratio between those two fractions is changed. After 240 min of mechanical activation, one more fraction below 0.1 μm is present in the sample. The agglomerates around 10 μm are in majority, with smaller particles gathered around them, making a minority in the mixture. Based on Fig. 2a, values of $d_{0.5}$ are: 11.67, 3.23, 5.93, 4.95, and 8.13 for Sh-0, Sh-30, Sh-60, Sh-240, and Sh-480, respectively, indicating that all values belonging to activated powders are lower than for non-activated ones.

Fig. 2b shows that all powders possess narrow distribution of particles, where maximums are: 0.416, 0.411, 0.443, 0.069, and 0.489 μm for Sh-0, Sh-30, Sh-60, Sh-240, and Sh-480, respectively, meaning that the powder activated for 240 min has nanocrystalline nature.

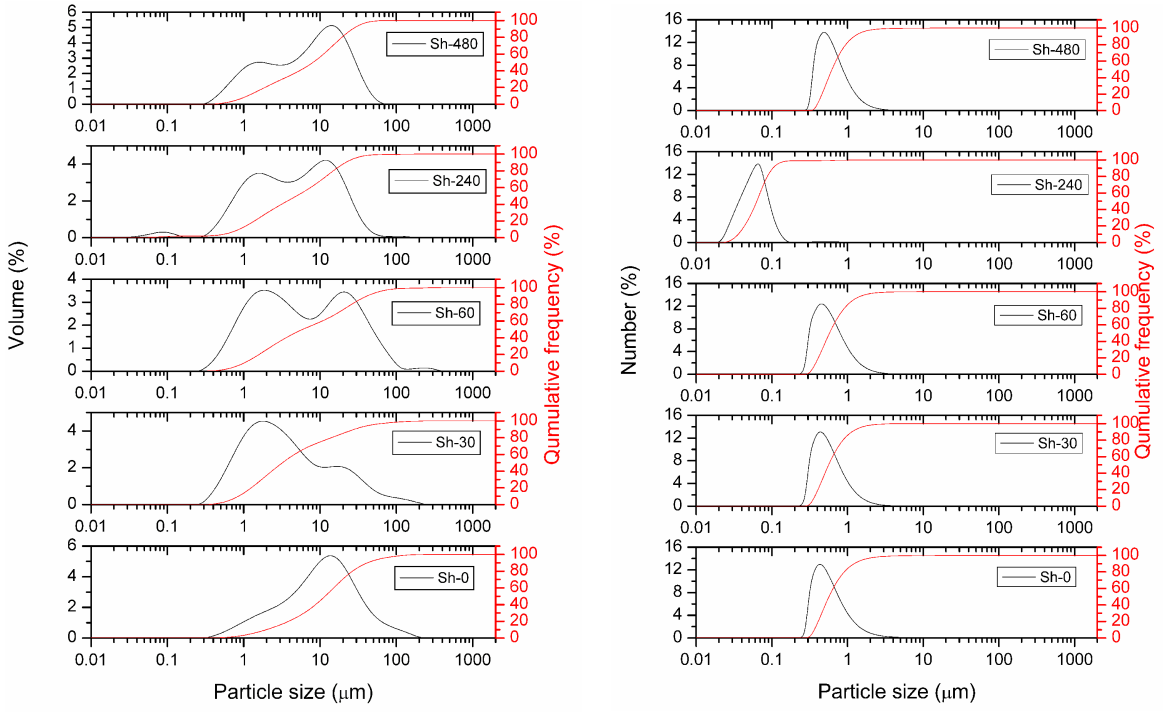

Figure 2. Particle size analysis of the starting powder and mechanically activated powders: a) distribution by volume, and b) distribution by number

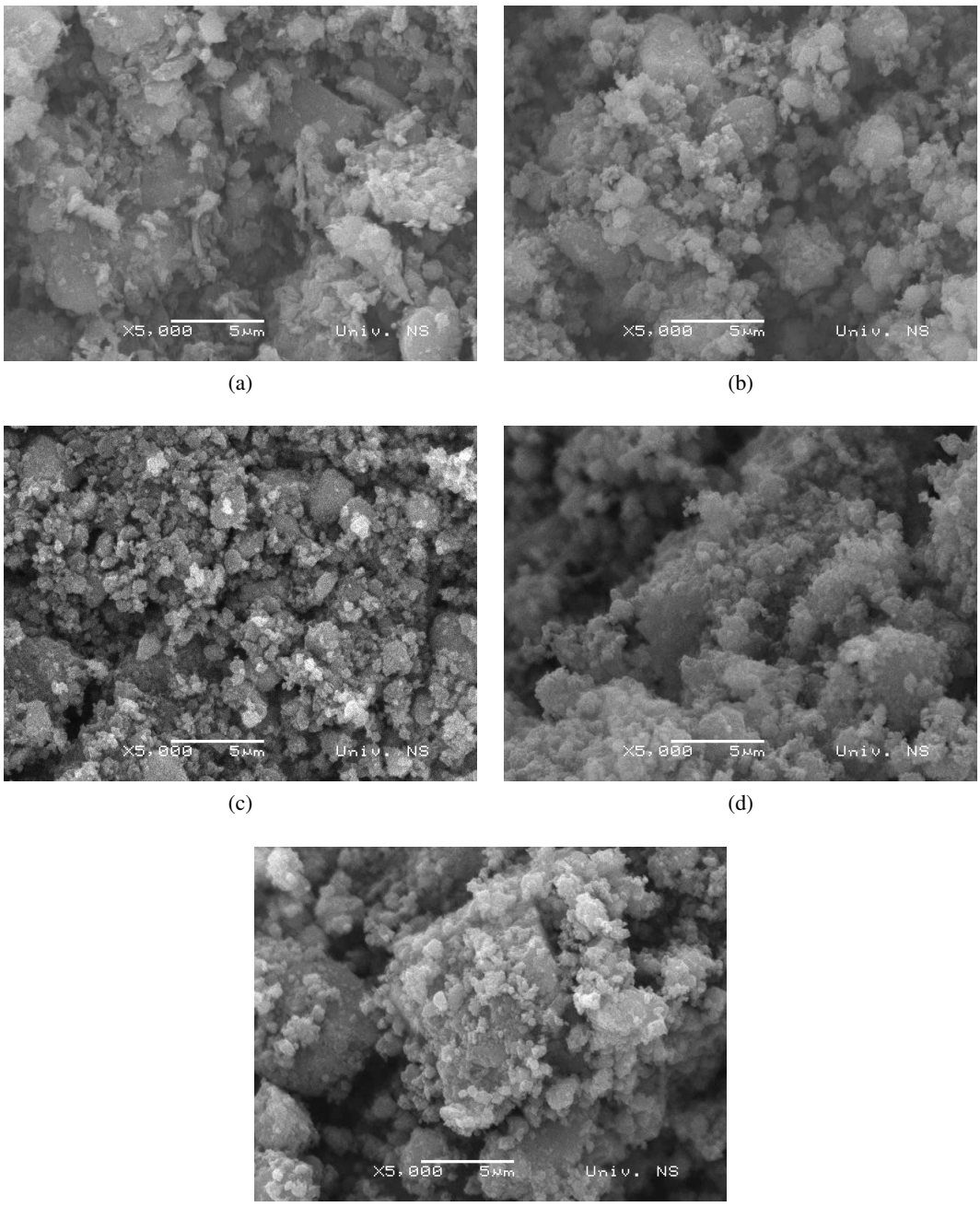

Figure 3. SEM micrographs of initial and activated samples: a) Sh-0, b) Sh-30, c) Sh-60, d) Sh-240 and e) Sh-480

Scanning electron micrographs of the initial and mechanically activated powders are presented in Fig. 3. Irregularly shaped particles and large agglomerates of $\geq$ 10 μm are present in the non-activated powder, as confirmed by the PSA measurement. The attrition of agglomerates and particles is noticed for Sh-30, while the most homogeneous distribution is noticed within the Sh-60 powder. A prolonged activation leads to the secondary agglomeration, clearly visible in Figs. 3d,e, where soft agglomerates in Sh-240 are covered with the smallest regularly shaped particles. This is very common, as the introduction of a high energy into a system with a prolonged milling time always leads to a drastically increased reactivity of powder particles.

At the beginning of the milling process, the powder particles become reactive, capable to form new phases, and then, with additional energy transfer, they are practically forced to make agglomerates. Those agglomerates could be a disadvantage during sintering [14].

Raman spectroscopy is known as an effective non-destructive approach, which gives detailed molecular-level information. Raman spectroscopy is widely used for the study of carbon in its various crystalline and allotropic modifications. Figure 4 presents Raman spectra of shungite carbon in range of 0–3500 cm^{-1}. It is known that the Raman spectra of amorphous carbon usually have two bands - G (graphite) band with the wavenumber of about 1560 cm^{-1} and D (diamond) band with the

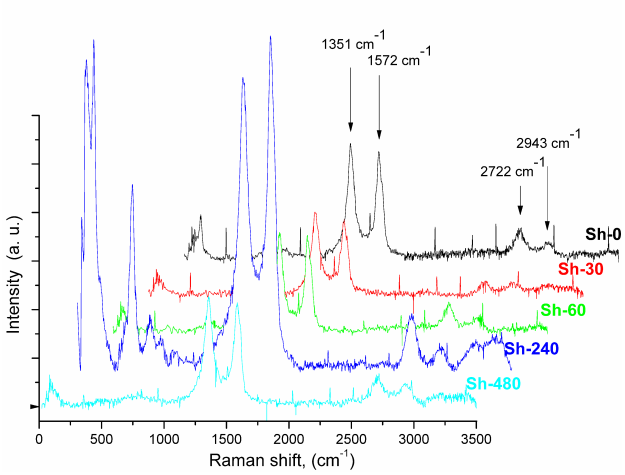

Figure 4. Raman spectra of non-activated and mechanically activated powders

wavenumber of about 1350 cm^{-1}, due to sp^2 bonds [15]. G band is conditioned by stretching pairs of sp^2 bonds in carbon rings and chains, and D band by changes in crystallographic axes La, Lc in carbon chains. The intensity of D band is a measure of structural disarrangement [16]. For investigated Sh-0 powders, bands are observed at 91, 1351, 1582, 2711, and 2943 cm^{-1}. Sharp Raman peaks at approx. 100 cm^{-1}, present in all samples, are common for lattice vibrations in crystals, La modes. All activated samples exhibit same peaks as the non-activated one. Raman spectra of shungite carbon are typical spectra of carbon polycrystals of graphite structure with small grains, and consist of two broad bands with maximums at 1355–1360 cm^{-1} and 1586–1605 cm^{-1}, so-called D and G bands [17]. In sample Sh-240, the slight shift toward lower intensities is noticed; the position of D and G bands is at 1343 and 1575 cm^{-1}, respectively. Depending on the structural state of carbon, in Raman spectra the width of lines and the ratio of D/G intensities change. Furthermore, in the spectra of CMRM activated for 240 min, one can see absorption band at 451 cm^{-1} which occurs in the spectra of nanoparticles, belonging to Si–O–Si vibrations. The oscillations in the region of 2722 and 2934 cm^{-1} in the spectra of CMRM powders indicate the structural closeness of shungite carbon to vitreous carbon. Finally, sample activated for 240 min exhibit nanostructural morphology. Major changes in crystal structure originated from intensive ball-milling are detected trough shifting of Raman intensities toward lower values [16].

Figure 5 presents DTA-TG curves for the non-activated powder, recorded in air and argon atmosphere. There is a strong exothermic effect at approximately 600 °C, originating from combustion of carbon, observed in the curve recorded in an air atmosphere [17]. The combustion reaction is followed by a mass loss of more than 36%, corresponding with the amount of C in the starting mixture (see Table 1). The mass loss remains unchanged with the change in the present atmosphere, approx. 40%, due to pyrolytic reaction that occurs in the absence of air.

However, DTA curve obtained in Ar atmosphere is different, without an exo-peak at 600 °C, but with one endo- and two other exo-peaks, see Fig. 5. The sample Sh-0 shows an endothermic peak, which starts below 100 °C with a maximum at around 192 °C, due to the removal of the remaining physiosorbed and chemisorbed water [18]. The first exo-peak at 850 °C and the other one at 1300 °C, correspond to $\gamma \rightarrow \alpha$ alumina phase transformation [19] and SiC formation [20], respectively.

The phase compositions of the non-activated and activated samples after the sintering process are presented in Figs. 6-10. The XRD pattern of the initial non-activated sample sintered at 800 °C for 2 h indicates that only one phase of alpha SiO_2 is dominant. The applied temperature is obviously too low for any reaction. The first peaks that correspond to SiC are detected after sintering at 1350 °C for 2 h in an Ar atmosphere, along with traces of unreacted SiO_2. A pure SiC phase is obtained after sintering at 1850 °C for 2 h in a vacuum. All sintered samples are very porous, with relative densities

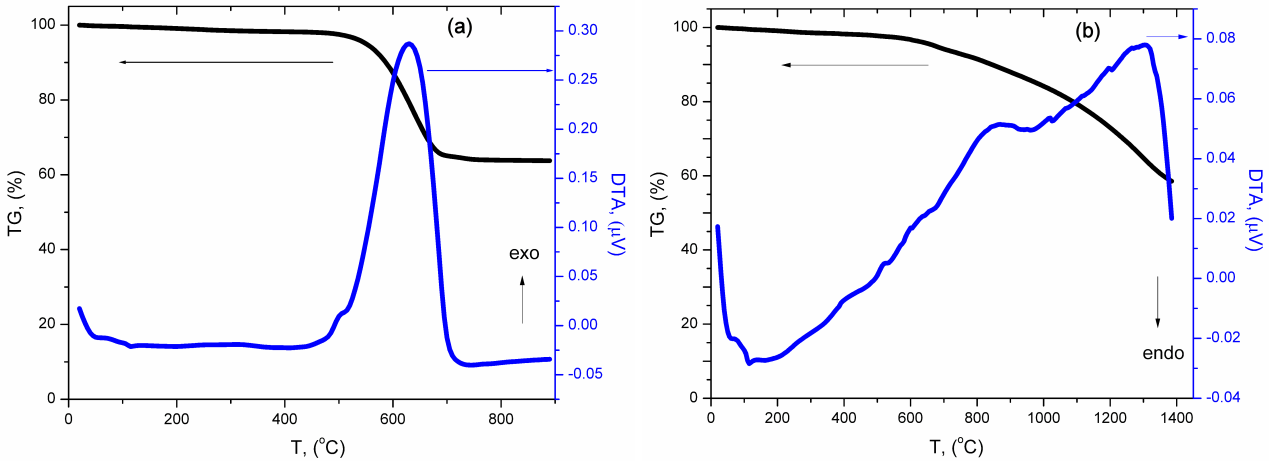

Figure 5. DTA-TG curves for non-activated Sh-0 powder in air (a), and in Ar atmosphere (b)

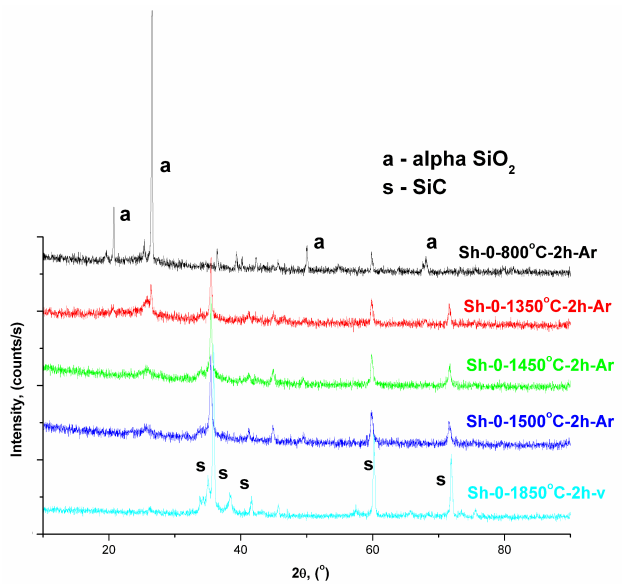

Figure 6. XRD patterns of Sh-0 powder sintered at various temperatures

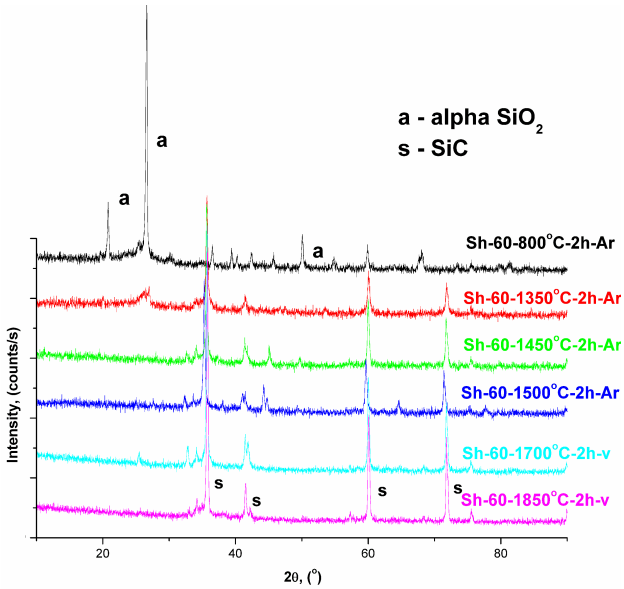

Figure 8. XRD patterns of Sh-60 powder sintered at various temperatures

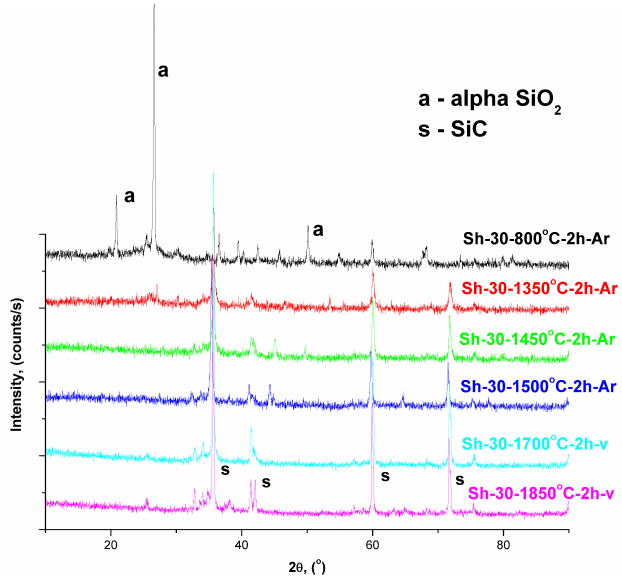

Figure 7. XRD patterns of Sh-30 powder sintered at various temperatures

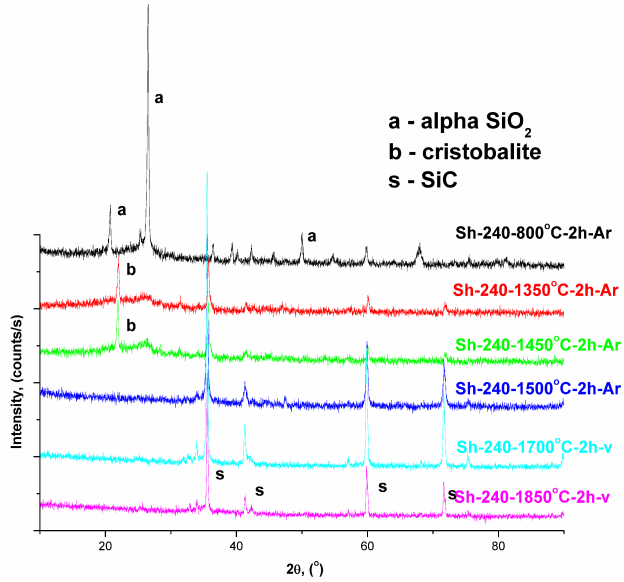

Figure 9. XRD patterns of Sh-240 powder sintered at various temperatures

below 20% TD (ρ_{TD} = 3.166 g/cm^3 for SiC). Identification of the obtained reflections was carried out using JCPDS cards (9009666 for α-SiO_2, 1010938 for β-SiO_2, and 900856 for SiC).

Very similar XRD patterns are observed after sintering of Sh-30 and Sh-60 powders (see Figs. 7 and 8). Pure SiC phases without any other phases are achieved after sintering at 1700 and 1850 °C for 2 h in a vacuum, with sharp and well crystallized reflections. The relative densities of the sintered samples are in the range from 18.6% TD, obtained for Sh-60 sintered at 1700 °C for 2 h in vacuum, to 21.4% TD, obtained for the same powder sintered at higher temperatures.

The XRD patterns of the samples activated for 240 and 480 min and sintered at 800 °C for 2 h indicate that only one phase of alpha SiO_2 is dominant, as in the previous cases. The XRD patterns of those samples after sintering at 1350 and 1450 °C for 2 h in Ar atmosphere indicate that β-modification of SiO_2 phase along with SiC reflections are present. Temperature of 1500 °C is needed for pure SiC phase to crystallize in the sample activated for 240 min and sintered. This represents the lowest temperature to obtain the pure phase in all investigated samples, probably due to the nanocrystalline structure after the milling process. As expected, with the increased sintering temperatures, pure silicon-carbide is noticed within samples, as well as higher relative densities, reaching the maximum values of 25.2 and 29.45% TD for Sh-240-1850-2h and Sh-480-1850-2h, respectively.

Real part of the complex relative permittivity (dielectric constant) of the samples, measured in the frequency range from 1 to 500 MHz, is shown in Fig. 11, while the results for the loss tangent are presented in Fig. 12. Both the relative permittivity and the loss tangent of the samples sintered at 1700 °C are substantially lower than for the samples sintered at 1850 °C. The sample Sh-240 has the highest relative permittivity and loss tangent of all samples sintered at 1700 °C for 2 h, while the sample Sh-60 has the highest relative permittivity and loss tangent of all samples sintered at 1850 °C for 2 h. This can be attributed to the homogeneous distribution and the smallest size of particles within the powder. The obtained relative permittivity and loss tangent values can be attributed to the polycrystalline structure, with electrically conductive grains and non-conductive grain boundaries, as well as high porosity [21, 22].

Lossy materials, like the sintered samples presented here, can be used in radiofrequency (RF) and microwave engineering as absorbers of electromagnetic waves, which can be implemented in the design of attenuators, matched loads and other similar components. SiC-based materials were considered and used for low-reflection terminations in waveguides [21,23] as well as

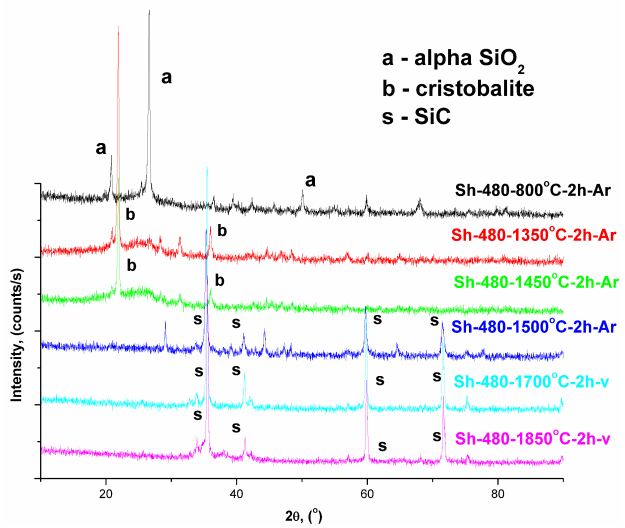

Figure 10. XRD patterns of Sh-480 powder sintered at various temperatures

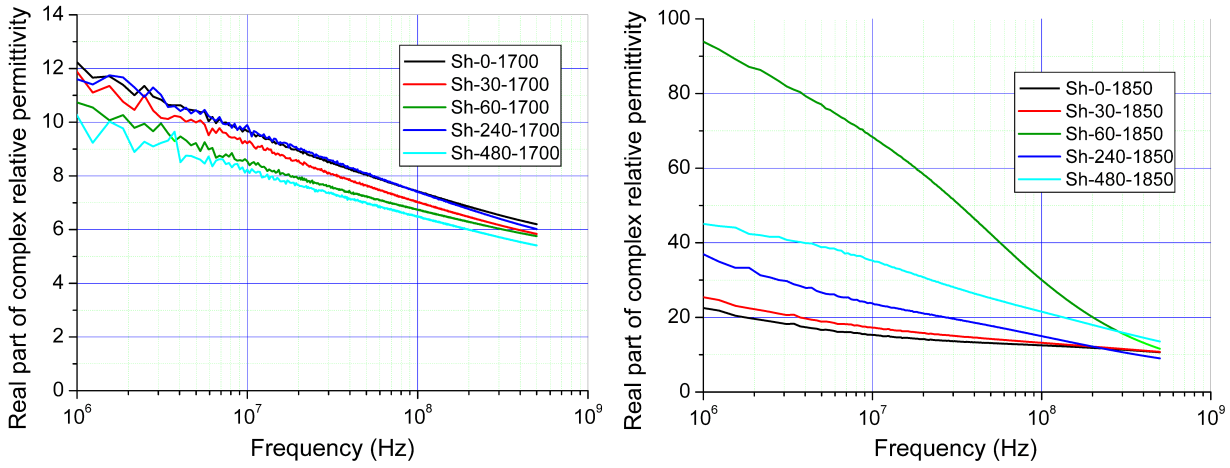

Figure 11. Real part of the complex relative permittivity of samples sintered for 2 h at: a) 1700 and b) 1850 °C

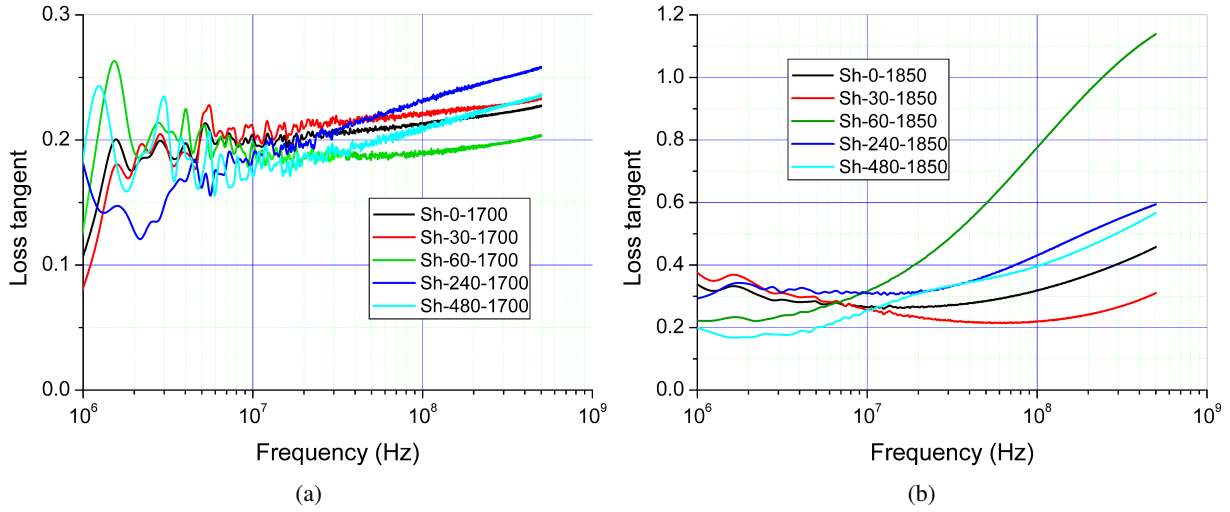

Figure 12. Loss tangent of samples sintered for 2 h at: a) 1700 and b) 1850 °C

for radar absorbers [24]. We investigated other possibilities of applications, using numerical simulators of electromagnetic structures [25]. All sintered samples are good as absorbers of plane waves if the ceramic material has the shape of an array of pyramids. These materials are also good as substrates for planar (printed) transmission lines used to design and fabricate matched microwave attenuators and low-reflection loads, with the reflection coefficient being −10 dB or lower. We have also established that transmission lines printed on Sh-240-1700 and Sh-60-1850 have the smallest dimensions for given attenuations, electrical lengths, and characteristic impedances, which is essential for miniaturization of microwave devices. This feature is due to the highest relative permittivity and loss tangent in the major part of the considered frequency range.

IV. Conclusions

In the present study, physico-chemical properties of a carbon-mineral rock material were investigated. The phase composition, microstructure, sinterability and electric properties of the initial and sintered materials were characterized systematically. The most important conclusions are:

1. The chemical composition of the initial powder consisted of over 52 wt.% of SiO_2 and the rest were C, Fe_2O_3, and Al_2O_3 components. No new phases were observed during milling.
2. SEM indicated that irregularly shaped particles and large agglomerates of around 10 μm are present in Sh-0. The attrition of agglomerates and particles was noticed for Sh-30, while the most homogeneous distribution was observed for Sh-60. The smallest particles were observed within the Sh-240 powder, as confirmed by PSA measurements.
3. DTA-TG curves for the non-activated powder, showed a strong exothermic effect at approx. 600 °C, originating from combustion of carbon, along with a mass loss of more than 36%, in air. During the heating regime in an Ar atmosphere, the sample Sh-0 showed an endothermic peak at 192 °C, due to the removal of the remaining physiosorbed and chemisorbed water. Besides mass loss of around 40%, curves possess two exo-peaks at 850 and 1300 °C, corresponding to $\gamma \rightarrow \alpha$ alumina phase transformation, and SiC formation, respectively.
4. The first traces of SiC are detected after sintering at 1350 °C for 2 h in an Ar atmosphere, along with traces of unreacted SiO_2. Temperature of 1500 °C represents the lowest value for obtaining pure SiC in Sh-240 sintered sample, due to the nanocrystalline structure.
5. All sintered samples are very porous. With the increased sintering temperatures, relative densities reached the maximum value of 29.4% TD for Sh-480-1850 for 2 h. The sintered samples have a large porosity and a polycrystalline structure, confirmed by Raman measurements, which strongly affects their electrical properties, resulting in a high relative permittivity and loss tangent. It is established that sintered samples can be used as an absorber of electromagnetic waves in various applications in microwave engineering.

Acknowledgement: The investigated mineral containing shungite is a donation from ART LINE SYSTEM doo from Novi Sad for scientific proposes. The authors acknowledge financial support from Ministry of Education, Science and Technological development of Serbia, Projects No. OI 172057 and III 45005. A part of experiments was conducted within DAAD scholarship project titled "Development of materials and manufacturing technologies for electric discharge machinable Zirconia-CNT/Graphene composites". The part of experiments was conducted within the following projects: NSF: HRD-1345219 and DMR-1523617 NASA: NNX09AV07A; GSF of CR: 17-05620S; MEYS of CR: CEITEC 2020 (LQ1601). The authors are grateful to Dr. Miodrag Mitrić for XRD measurement, Dr. Smilja Marković for PSA, Dr. Darko Kosanović for mechanical activation, Prof. Dr. Slavko Mentus for DTA-TG measurements, and Miloš Bokorov for SEM measurements.

References

1. M.V. Avdeev, T.V. Tropin, V.L. Aksenov, L. Rosta, V.M. Garamus, N.N. Rozhkova, "Pore structures in shungites as revealed by small-angle neautron scattering", *Carbon*, **44** (2006) 954–961.
2. P.R. Buseck, L.P. Galdobina, V.V. Kovalevski, N.N. Rozhkova, J.W. Valley, A.Z. Zaidenberg, "Shungites: the C-rich rocks of Karelia, Russia", *Can. Mineral*, **35** (1997) 1363–1378.
3. E.N. Grigorieva, N.N. Rozhkova, "Shungite carbon behavior in the modelling reactions of coal thermal decomposition", *J. Appl. Chem.*, **73** (2000) 600–605.
4. A.Z. Zaidenberg, "Shungite influence on the water chemistry", in *Twenty-third Biennial Conference on Carbon (Carbon'97), Extended Abstracts*, Pennstate II (1997) 118–119.
5. N.N. Rozhkova, "Shungite-a carbon mineral filler for polymeric composite materials", *Compos. Interface*, **8** (2001) 307–312.
6. N.N. Rozhkova, I. Iordache, A.M. Bondar, I. Pasuk, B. Rand, "Natural and synthetic ceramics with shungite carbon", pp. 73–75 in *Extended abstracts conference on Carbon*, Beijing, 2002.
7. O.W. Mosin, "Shungite-natural material for nanotechnology", *Nano News Network* (2008), in Russian.
8. I.F. Kurunov, "Mechanism and theoretical evaluation of coke replace by shungite in blast furnaces", *Metallurgy*, **7** (2003) 20–27.
9. O. Mosin, I. Ignatov, "The structure and composition of natural carbonaceous fullerene containing mineral shungite", *Int. J. Adv. Sci. Technical Res.*, **3** [6] (2013) 9–21.
10. N. Obradović, N. Đorđević, A. Peleš, S. Filipović, M. Mitrić, V.B. Pavlović, "The influence of compaction pres-

sure on the density and electrical properties of cordierite-based ceramics", *Sci. Sinter.*, **47** (2015) 15–22.
11. A. Gubernat, W. Pichor, R. Lach, D. Zientara, M. Sitarz, M. Springwald, "Low-temperature sunthesis of silicon carbide powder using shungite", *Bol. Soc. Esp. Ceram. V.*, **56** [1] (2017) 39–46.
12. A. Đorđević, J. Dinkić, M. Stevanović, D. Olćan, S. Filipović, N. Obradović, "Measurement of permittivity of solid and liquid dielectrics in coaxial chambers", *Microwave Rev.*, **22** [2] (2016) 3–9.
13. N. Obradović, N. Đorđević, S. Filipović, S. Marković, D. Kosanović, M. Mitrić, V. Pavlović, "Reaction kinetics of mechanically activated cordierite based ceramics studied via DTA", *J. Therm. Analy. Calorim.*, **124** [2] (2016) 667–673.
14. N. Obradović, S. Filipović, N. Đorđević, D. Kosanović, V. Pavlović, D. Olćan, A. Đorđević, M. Kachlik, K. Maca, "Microstructural and electrical properties of cordierite-based ceramics obtained after two-step sintering technique", *Sci. Sinter.*, **48** (2016) 157–165.
15. A.C. Ferrari, J. Robertson, "Interpretation of Raman spectra of disordered and amorphous carbon", *Phys. Rev. B*, **61** [20] (2000) 14095–14107.
16. S.A. Efremov, S.V. Nechipurenko, M.K. Kazankapova, B. Washington, Kh.S. Tassibekov, M.K. Nauryzbaev, "Physico-chemical characteristics of shungite rock of Kazakhstan", *Eurasian Chem. Tech. J.*, **15** [3] (2013) 241–249.
17. Q. Zhang, H. Liu, X. Zhang, H. Xing, H. Hu, H. Yao, "Novel utilization of conditioner CaO for gas pollutants control during co-combustion of sludge and coal", *Fuel*, **206** (2017) 541–545.
18. A.A. Taromi, S. Kaliaguine, "Synthesis of ordered mesoporous γ-alumina - Effects of calcination conditions and polymeric template concentration", *Micropor. Mesopor. Mater.*, **248** (2017) 179–191.
19. S. Lamouri, M. Hamidouche, N. Bouaouadja, H. Belhouchet, V. Garnier, G. Fantozzi, J.F. Trelkat, "Control of the γ-alumina to α-alumina phase transformation for an optimized alumina densification", *Bol. Soc. Esp. Ceram. V.*, **56** (2017) 47–54.
20. Z. Omidin, A. Ghasemi, S.R. Bakhshi, "Synthesis and characterization of SiC ultrafine particles by means of sol-gel and carbothermal reduction methods", *Ceram. Int.*, **41** (2015) 5779–5784.
21. Y. Takeuchi, T. Abe, T. Kageyama, H. Sakai, "RF dielectric properties of SiC ceramics and their application to design of HOM absorbers", pp. 1195–1197 in *Proceedings of 2005 Particle Accelerator Conference*, Tennessee, USA, 2005.
22. A.R. Đorđević, D.I. Olćan, N. Obradović, V. Paunović, S. Filipović, V.B. Pavlović, "Electrical properties of magnesium titanate ceramics post-sintered by hot isostatic pressing", *Sci. Sinter.*, **49** (2017) 373–380.
23. J. Guo, F. Fors, J. Henry, R. A. Rimmer, H. Wang, H.-W. Glock, A. Neumann, A. Tsakanian, A. Velez, "Development of waveguide HOM loads for bERLinPro and BESSY-VSR SRF cavities", pp. 1160–1163 in *Proceedings of IPAC2017*, Copenhagen, Denmark, 2017.
24. J.-H. Ha, S. Lee, J.R. Choi, J. Lee, I.-H. Song, T.-J. Chung, "A self-setting particle-stabilized porous ceramic panel prepared from commercial cement and loaded with carbon for potential radar absorbing applications", *Process. Appl. Ceram.*, **12** [1] (2018) 86–93.
25. A.R. Djordjević, M.B. Baždar, R.F. Harrington, T.K. Sarkar, "LINPAR for Windows: Matrix Parameters for Multiconductor Transmission Lines", Artech House, Boston, 1999.